Cellulose (2018) 25:4577–4589
https://doi.org/10.1007/s10570-018-1875-3

ORIGINAL PAPER

Cellulose nanofibril-reinforced composites using aqueous dispersed ethylene-acrylic acid copolymer

Abhijit Venkatesh · Johannes Thunberg · Tobias Moberg · Maria Klingberg · Lars Hammar · Anna Peterson · Christian Müller · Antal Boldizar

Received: 23 October 2017 / Accepted: 28 May 2018 / Published online: 9 June 2018

Abstract In order to explore the reinforcing capabilities of cellulose nanofibrils, composites containing high contents of cellulose nanofibrils were prepared through a combination of water-assisted mixing and compression moulding, the components being a cellulose nanofibril suspension and an aqueous dispersion of the polyolefin copolymer poly(ethylene-*co*-acrylic acid). The composite samples had dry cellulose nanofibril contents from 10 to 70 vol%. Computed tomography revealed well dispersed cellulose fibril/fibres in the polymer matrix. The highest content of 70 vol% cellulose nanofibrils increased the strength and stiffness of the composites by factors of 3.5 and 21, respectively, while maintaining an elongation at break of about 5%. The strength and strain-at-break of cellulose nanofibril composites were superior to the pulp composites at cellulose contents greater than 20 vol%. The stiffness of the composites reinforced with cellulose nanofibrils was not higher than for that of composites reinforced with cellulose pulp fibres.

A. Venkatesh · J. Thunberg (✉) · T. Moberg · M. Klingberg · L. Hammar · A. Boldizar
Department of Industrial and Materials Science, Chalmers University of Technology, 412 96 Gothenburg, Sweden
e-mail: johannes.thunberg@chalmers.se

T. Moberg
Wallenberg Wood Science Center, 412 96 Gothenburg, Sweden

A. Peterson · C. Müller
Department of Chemistry and Chemical Egineering, Chalmers University of Technology, 412 96 Gothenburg, Sweden

Graphical Abstract

Keywords Cellulose nanofibrils · Cellulose composite · Amphiphilic co-polymer · Latex · Nanocomposite · Direct mixing · Rheology

Introduction

Natural cellulosic fibres such as wood pulps are well known reinforcing agents in composites and the high strength and large aspect ratio of nano-scale cellulose fibrils make them suitable as reinforcement in composite materials (Berglund and Peijs 2010; Oksman et al. 2016). Recent developments in cellulose pulp processing have made nano-sized cellulose fibrils commercially available (Saito et al. 2007). Since cellulose is one of the most abundant organic polymer in the world, it has the potential to be an inexpensive reinforcing filler material in thermoplastics. A major drawback of using cellulose nanofibrils (CNF) as reinforcement in thermoplastics is however the difference in hydrophilic nature between cellulose and the usually hydrophobic matrix phase polymer. Moreover, it can be argued that dewatering and drying of cellulose nanomaterials promotes irreversible bonding between nanofibrils, as discussed in Fernandes Diniz et al. (2004). This incompatibility can affect the mixing of the cellulose in the matrix and can lead to aggregation of cellulose fibre/fibrils resulting in a non-uniform thermoplastic composite (Ariño and Boldizar 2012). Insufficient compatibility can also result in poor fibre–matrix adhesion, leading to poor stress transfer and inferior mechanical properties. In addition, the low thermal degradation temperature of cellulose limits the range of processing temperatures and the selection of applicable polymer matrices. Common matrices used in melt extrusion of CNF are polyesters such as poly(lactic acid) (PLA) (Jonoobi et al. 2010), due to its renewable origin and biodegradability. Other common matrices used are polyethylene and polypropylene (Boldizar et al. 1987), which have relatively low melting temperatures and are common bulk polymers.

To create well dispersed CNF composite materials, methods that focus mainly on cellulose surface chemistry have been used (Dufresne 2017). These include grafting hydrophobic compounds to the cellulose surface to make the fibrils more hydrophobic, often combined with a solvent exchange step (Siqueira et al. 2009; de Menezes et al. 2009). Surfactants or the surface adsorption of amphiphilic co-polymers have also been used to improve the dispersion and compatibility of the CNF in the polymer matrix (Volk et al. 2015). These methods have been effective, but the use of non-polar solvents and multiple reaction steps may limit their industrial relevance.

The method of solvent casting CNF together with a water-soluble polymer is known to yield a well dispersed composite with excellent mechanical properties (Sehaqui et al. 2011; Srithep et al. 2012). However, the use of a water-soluble matrix polymer makes the resulting composite moisture-sensitive. To avoid this, an insoluble aqueous-dispersed polymer can be used to solvent cast composites. This approach is not entirely new, early efforts include the use of cellulose nanocrystals in combination with natural

rubber latex as a matrix phase (Favier et al. 1995). Water-assisted mixing of CNF and micrometer-sized PLA latex has been used to create fully biodegradable composites with improved tensile properties (Larsson et al. 2012). More recently, a aqueous dispersion of an elastomeric co-polymer using poly(ethylene-acrylic acid) as stabilizing surfactant was used to create CNF composite films with improved tensile stiffness (Maia et al. 2017).

In the present work, poly(ethylene-*co*-acrylic acid) (EAA) reinforced with unmodified CNF was mixed according to the water-assisted method, with the purpose to explore the possibility to disperse high contents of CNF in a polymer matrix. The EAA polymer was selected mainly due to it being insoluble in water and having the ability to form a stable aqueous dispersion. Also, this modified polyethylene had previously shown good adhesion and compatibility with regenerated cellulose (Saarikoski et al. 2012). Composites with up to 70 vol% dry content CNF could be made. To better understand the general capability of CNF to reinforce a polymer matrix, the thermal and mechanical properties were studied in comparison with those of plain cellulose pulp composites. The cellulose pulp selected for comparison consisted mainly of spruce sulphite and was of a highly beaten type with a similar surface structure as the CNF used.

Methods

Materials

Poly(ethylene-*co*-acrylic acid) (EAA) dispersion with a 20 wt% solids content was obtained from BIM Kemi AB, Sweden. The EAA polymer had an acrylic acid content of 15%, a density of 0.994 g/cm^3, a melting point of 88 °C and a melt flow rate of 36 g/10 min (ISO 1133, 190 °C, 2.16 kg), according to the supplier. The dispersed EAA was neutralized to its ionomer form with NaOH during the dispersing process. The pH of the EAA dispersion was 9.7. CNF paste made from spruce sulphite pulp was kindly provided by Borregaard AS, Norway. The CNF had a solids content of 10 wt% in water. The CNF had a Klason lignin content of 3.2 wt%, a hemicellulose content (arabinoxylan and galactoglucomannan) of 2.8 wt% and a cellulose content of 94 wt%. These contents were estimated from monosaccharide carbohydrate analysis. The cellulose fibre pulp used was a highly beaten never-dried bleached softwood mixture of 80% spruce sulphite and 20% spruce sulphate pulp, kindly provided by Nordic Paper Seffle AB, Sweden. The pulp had a Klason lignin content of 1.9 wt%, a hemicellulose content of 17 wt% and a cellulose content of 80 wt%.

Rheological measurements

The rheological properties of the suspensions were measured using an Anton Paar MCR702, Twin-drive shear rheometer (Graz, Austria). The suspensions studied were the CNF paste, with a dry content of 10 wt% and additionally the CNF–EAA suspensions containing 0.7 wt% CNF and 1.8 wt% CNF, respectively. The linear viscoelastic range of these suspensions was characterized through oscillatory shear strain measurements in the range of 0.01–100% strain and a frequency of 1 Hz. The steady shear flow was investigated in the shear rate range of 0.1–100 s^{-1}, the measurements being performed at 25 °C using a cone-plate fixture. The cone-plate geometry had a diameter of 25 mm, a cone angle of 2° and a gap distance of 0.106 mm. Temperature sweeps were performed on the 70 and 10 vol% CNF–EAA suspensions from 27 to 90 °C at a frequency of 1 Hz and a strain amplitude of 0.2%. A parallel-plate fixture with a plate diameter of 15 mm and a gap distance of 0.5 mm was used for these measurements and silicone oil was used to reduce the evaporation of water.

Fibre analysis

The fibre length and width was determined according to Tappi standard T271 using a Kajaani FS300 fibre analyser (Metso Automation, Finland), where fines content is based on the centerline length. Fibre length and width are reported as mean values based on approximately 30,000 fibre pieces.

Dynamic light scattering

The hydrodynamic diameter of the EAA particles in suspension was measured using a Malvern Instruments Zetasizer ZEN3600. The data reported is the z-average from cumulant fit. The EAA dispersion was diluted to 0.01 wt% with deionized water and

sonicated for 10 min. Measurements were conducted in a standard quartz cuvette at room temperature.

Composite manufacture

EAA dispersion was added to CNF paste or pulp to obtain the intended volume fractions of cellulose. The mixtures had a solids content of 2.5–4.5 wt% cellulose, and excess of water was added to achieve a total water content of $96 \pm 1\%$. These suspensions were then mixed at room temperature in an L&W pulp disintegrator (Lorentzen & Wettre, Sweden) for 60,000 revolutions at 2900 rpm. Volume fractions were calculated assuming a cellulose density of 1.5 g/cm^3 and an EAA density of 0.994 g/cm^3. The mixed cellulose and EAA suspensions were dried at room temperature to about 0.1 mm thick sheets. Approximately 12 g of the dry sheets were stacked and compression moulded to composite plates with an area of 100×100 mm^2 and a thickness of about 1 mm using a Bucher–Guyer KHL 100, Switzerland. Stacks of dry sheets were placed in the open mould tempered at 105 °C. The mould was then closed and a pressure of 20 bar was applied until the distance between the mould halves had stabilized, which took approximately 5 min. The pressure was then raised to 500 bar and the mould was cooled to 30 °C, which took about 2 min. Finally, with the mould cooling turned off, the mould temperature was allowed to increase to 40 °C, which took about 1 min. The pressure was then released and the sample was removed from the mould.

Microscopy and tomography

Dried CNF paste was studied with a LEO Ultra 55 FEG Scanning Electron Microscopy (SEM). Samples were goldsputtered in vacuum for 80 s at 10 mA, to give a gold coating approximately 10 nm thick. The atomic force microscope (AFM) used was a Nanoscope IIIa with a type G scanner (Digital Instruments Inc.), with a Micro Masch silicon cantilever NSC 15. The measurements were performed in air and in the tapping mode. The 3D data of the internal structure of composites were scanned with a Zeiss Xradia XRM520 X-ray tomograph. The scanned volume were reconstructed to a size of 1 μm^3/voxel. Graphs of voxel gray scale were generated with the ImageJ software. 3D images of composite microstructure is based on surface reconstructions made in the software 3D slicer.

Differential scanning calorimetry

Thermograms were prepared by Differential Scanning Calorimetry (DSC), using a Perkin Elmer DSC7 from 10 to 250 °C. The scan rate was 10 °C/min and the sample mass was approximately 10 mg. Peak deconvolution was done using a three-term Gaussian function. The crystallinity of the EAA matrix was calculated using the Eq. 1.

$$X_c = \frac{\Delta H_c}{w_{EAA}\Delta H_0} \quad (1)$$

Here, ΔH_c is the specific heat of fusion of the composite, w_{EAA} is the mass fraction EAA of the sample and ΔH_0 is the specific heat of fusion for a polyethylene crystal (277.1 J/g) (Brandrup et al. 1999).

Dynamic mechanical thermal analysis

The viscoelastic properties of composites were evaluated using dynamic mechanical thermal analysis (DMTA). The measurements were performed with a Rheometrics Solids Analyzer RSA II at a frequency of 1 Hz, a heating rate of 3 °C/min and a strain amplitude between 0.1 and 0.15%. The temperature range used was -80 °C to 110 °C. The sample thickness varied between 0.8 and 1 mm and the width between 4 and 7 mm. The samples were measured in tension within the linear viscoelastic range. Prior to the temperature sweep, a strain sweep was performed for each sample series at room temperature.

Tensile testing

The Young's modulus (E), stress at break (σ_b) and elongation at break (ε_b), were evaluated in accordance with ISO 527-3. Samples were cut into dumb-bell shapes having a width of 4 mm and a thickness of approximately 1 mm and conditioned for at least 2 days at 23 ± 2 °C and $50 \pm 5\%$ relative humidity (RH) prior to testing, The tensile measurements were also made at 23 ± 2 °C and $50 \pm 5\%$ RH, with a Zwick Z1/Roell with a grip separation of 40 mm and the crosshead speed was 6 mm/min. A Zwick Eye UI 1540M video extensometer was used, with an initial gauge

length of 20 mm. A load of 0.1 N was applied before measurement. The tensile stiffness measured was compared to the Cox–Krenchel model according to Eq. 2.

$$E_c = \eta_d E_f \left(1 - \frac{\tanh\left(\frac{\beta l}{2}\right)}{\frac{\beta l}{2}}\right)\phi + (1-\phi)E_m \qquad (2)$$

where

$$\beta^2 = \frac{E_m/(1+\nu_m)}{r^2 E_f \ln\left(\frac{R}{r}\right)} \qquad \text{and} \qquad R = \sqrt{\frac{\pi r^2}{4\phi}}$$

E_m, E_f and E_c are the the elastic moduli of the EAA matrix, the cellulose fibre and the composite, respectively (Cox 1952; Thomason and Vlug 1996). E_m was measured to be 0.29 GPa and E_f was set to 21 GPa for cellulose fibres (Ehrnrooth and Kolseth 1984) and 32 GPa for the CNF (Tanpichai et al. 2012). ϕ is the volume fraction of cellulose and η_d is a orientation factor which was assumed to be 3/8 corresponding to a random in-plane fibre orientation (Thomason and Vlug 1996). The Poisson ratio, ν_m for the EAA matrix was assumed to be 0.3 and r is the fibre radius. Fibre dimensions were taken from the results of the fibre analysis. For CNF composites, a diameter of 18.4 µm and a length of 0.34 mm were used as the fibre analysis neglects both the pulp fines and the cellulose fibrils. For pulp composites, a diameter of 27 µm and a length of 1.3 mm were used.

The effective stiffness of CNF ($E_{f,l}$) was calculated using the method of Ansari et al. (2014), through the Halpin–Tsai model.

$$E_{f,l} = \frac{\frac{3}{8}\left(E_c - \frac{5}{8}E_T\right) - E_m(1-\phi)}{\phi} \qquad (3)$$

where

$$E_T = E_m\left(\frac{1+2\eta\phi}{1-\eta\phi}\right) \qquad \text{and} \qquad \eta = \frac{E_{f,t} - E_m}{E_{f,t} + 2E_m}$$

The transverse fibre modulus in Eq. 3 $E_{f,t}$ was set to 15 GPa (Diddens et al. 2008).

Results and discussion

Rheological properties

The shear storage modulus, (G′) at 1 Hz is shown as a function of the shear strain in Fig. 1a. The graph clearly shows a difference in G′ between the CNF paste and the CNF–EAA suspension with a water content of 96 ± 1 wt%. The lower G′ of the CNF–EAA suspensions was expected, due to the reduction in CNF concentration by the addition of EAA dispersion and the excess of water. The transition from the linear viscoelastic region to the non-linear region increased with decreasing CNF concentration, the addition of EAA and the excess of water as expected (Quennouz et al. 2015). The critical strain value, indicated by the drop in storage modulus, increased from 1.1% for the CNF paste to 2.3% for the CNF–EAA suspension with 0.7 wt% CNF dry content. These critical strains measured were estimated to corresponds to critical stress values of around 250, 7.6 and 2.4 Pa for the CNF paste, the 1.8 and 0.7 wt% suspensions respectively, and was coupled to the yield stress of the samples. Interestingly, the CNF content in the suspensions did not appear to affect the slope in the region of shear thinning. This observation was in contrast to previous work by Naderi et al. (2014), who showed an increase in the slope after the linear viscoelastic range with increasing CNF content of the suspension. Furthermore, it was here seen that the loss modulus (G″) was lower than the storage modulus G′ up to about 6 % strain indicating the more prominent elastic character of the CNF–EAA suspensions. Figure 1b shows the steady shear viscosity as a function of shear rate. A decreasing shear viscosity with increasing shear rate was observed, in agreement with earlier work (Moberg and Rigdahl 2012). The shear viscosity deceased with decreasing CNF content as expected. The viscosity could not be measured on the CNF paste at shear rates above 5 s^{-1} because of slippage between the sample and the cone-plate fixture. Figure 2 shows the G′ as a function of temperature for the CNF–EAA suspensions with 0.7 and 1.8 wt% CNF dry content, respectively. The high water content (96 ± 1%) in both the suspensions limited the temperature range of the experiments due to the evaporation of water, as indicated by the increase in G′ with temperature. The CNF–EAA suspension with 0.7 wt% CNF dry content

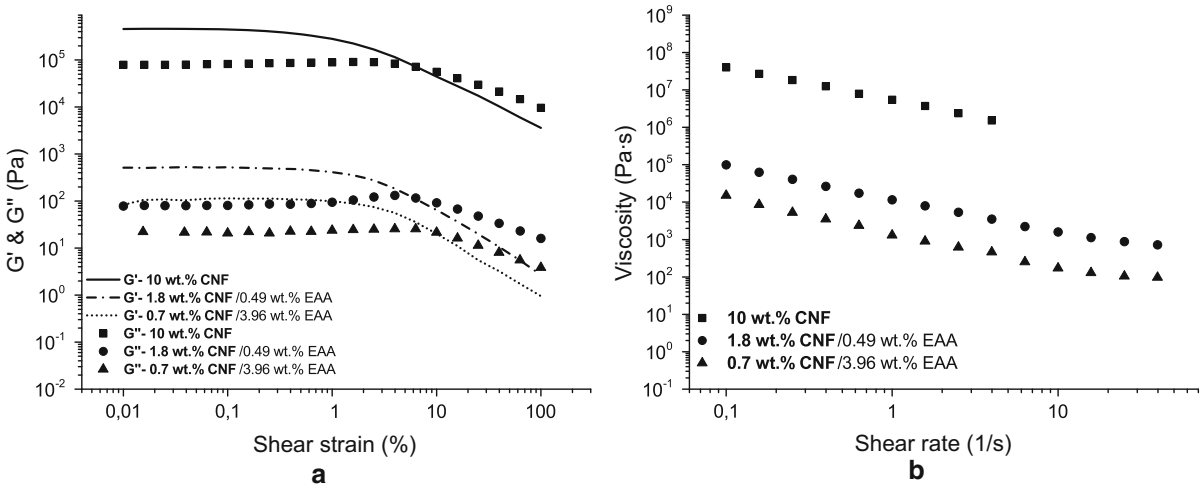

Fig. 1 **a** The dynamic shear storage modulus (G′, solid line) and the shear loss modulus, (G″, dashed line) as a function of shear strain and **b** the steady shear viscosity as a function of shear rate for CNF paste and CNF–EAA suspensions with 1.8 and 0.7 wt% CNF dry contents

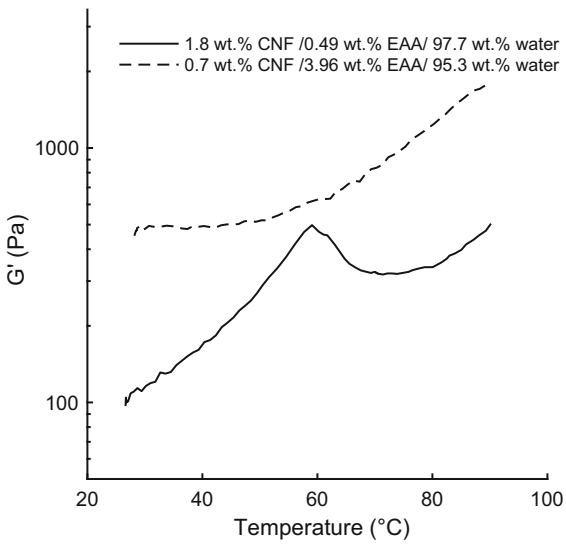

Fig. 2 The variation of dynamic shear storage modulus (G′) as a function of temperature for CNF–EAA suspensions with 1.8 and 0.7 wt% CNF dry contents

and 3.95 wt% EAA showed a peak in G′ at 59 °C, which is close to the first melting point of EAA. This peak suggests that the increase in G′ could be related to morphological changes in the EAA dispersion such as flocculation or coalescence, rather than just evaporation, at these temperatures. The peak was observed only in the sample with 0.7 wt% CNF dry content due to the high EAA concentration in the sample.

Cellulose and EAA morphology

Fibre analysis showed that fibres or large fibre fragments were still present in the CNF starting material. These fibres were however shorter than those in the pulp (Table 1). The large fibre fragments present in the CNF were probably the result of an incomplete fibrillation process. The fibrillated nature of the CNF was reflected in the fines content, see Table 1, which was much higher for the CNF than for the highly beated pulp.

The microstructure of the CNF used in this work is shown in Fig. 3a. Scanning electron microscopy revealed that the cellulose fibrils of the studied CNF had diameters and lengths largely on the micrometer scale. The smallest fibrils present in the CNF had diameters on the nanoscale (< 100 nm) as shown by AFM (Fig. 3b). The CNF appears to be a mixture of fibres, micro- and nanofibrils. The relative contents of these fibres, micro- and nanofibrils could not be determined, since none of the analysis techniques

Table 1 Fibre analysis of CNF and pulp

Cellulose type	Length (mm)	Width (μm)	Fines (%)
CNF	0.34	18.4	78.0
Pulp	1.36	24.4	11.9

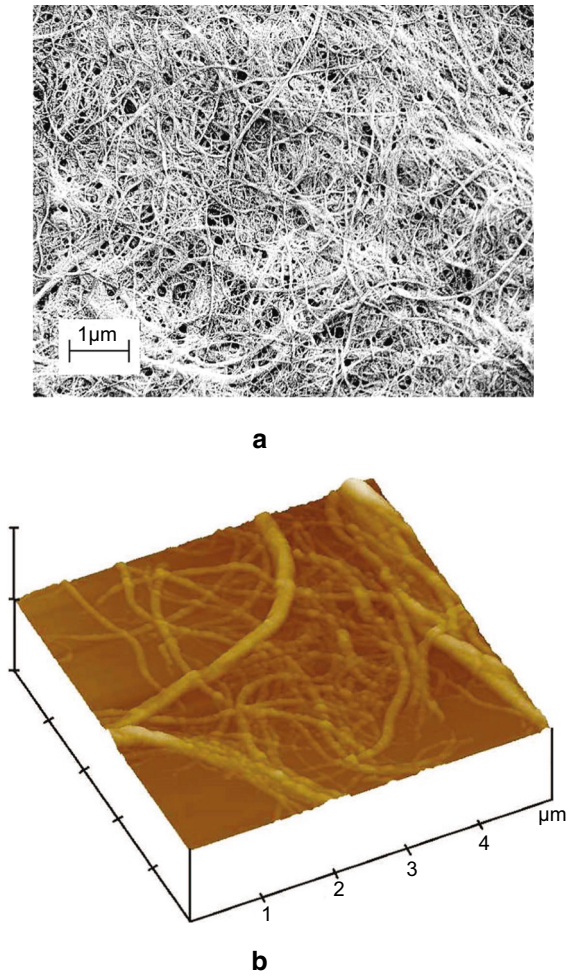

Fig. 3 Scanning electron micrograph of **a** dried CNF and **b** AFM image of dried CNF

covered the whole size range of the CNF material. The EAA dispersion used to make the composites was milky in appearance and the mean particle size was 50 nm, determined by dynamic light scattering. This particle size was considerably smaller than other micrometer sized latex dispersions that have been used to produce CNF composites (Larsson et al. 2012).

Composite microstructure

The microstructure of the cellulose-EAA composites was determined using X-ray microtomography with a reconstructed voxel size of 1 μm^3/voxel. Figure 4a shows the number of volume elements against the voxel gray scale for the EAA–CNF-20 composite material containing 20 vol% cellulose. As, the gray scale corresponds to the density of the material, three distinct phases could be distinguished. It was indicated that the phase with the highest voxel density corresponded to cellulose fibres and fibrils, since fibrous micro-structures were clearly seen in Fig. 4b. The volume fraction of the high density phase was however smaller than the total cellulose fraction of the composite, which suggests that the medium density phase was a mixture of EAA and cellulose fibrils smaller than the voxel size, 1 μm^3/voxel. The third distinguishable phase had a low density, suggesting purely amorphous EAA or voids. In Fig. 4b, the high density fibre/fibril phase and the low density phase are shown together. Interestingly, the low density phase was situated on fibre/fibril surfaces and inside the lumen of fibres. These findings indicate a low density inter-phase near the cellulose surface. In Figure 5b it can be seen that a low density phase also existed in the pulp–EAA composites. In the pulp–EAA composite, this phase was also situated close to the fibre surface and inside the lumen of fibres. The volume fraction of 13% for the high density fibre phase in the pulp–EAA composite with 20 vol% pulp content indicates that there were small fibril elements in the pulp that fall below the detection limit of X-ray microtomography. These undetected cellulose fibrils were probably included in the medium density phase.

Thermal properties

The semi-crystalline nature of EAA can be seen in the thermograms in Fig. 6. Multiple endothermic melting peaks were detected in the temperature interval 50–90 °C. A second heating after cooling at 10 °C/min generated a more distinct melting peak at about 88 °C, consistent with the melting temperature of non-isothermally crystallized EAA (Zhang et al. 2009). For ionomers such as neutralized EAA, it is understood that the low temperature endotherm arises due to the gradual formation of thin crystals at room temperature after primary crystallization (Loo et al. 2005). The multiple melting peaks in all the samples after compression moulding indicated that thin crystals had formed. The melting peaks could be described by a three-term Gaussian function (Fig. 6a). The crystallinity of these two melting regions are shown in Table 2. The secondary crystallinity of EAA (X_{c1} in

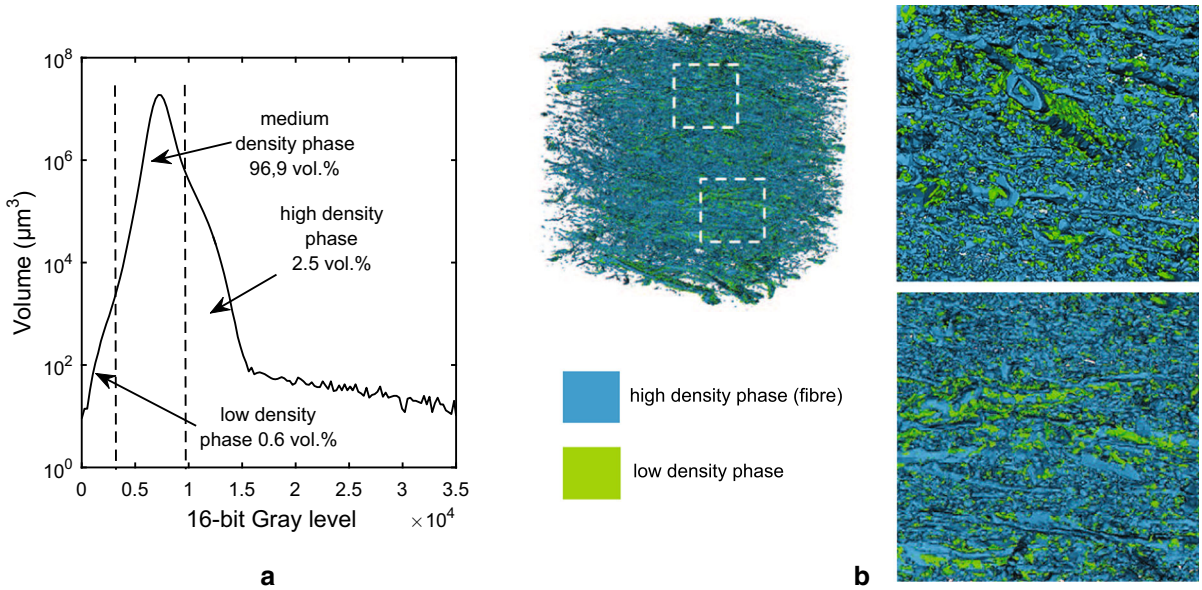

Fig. 4 EAA–CNF-20 **a** X-ray microtomography data showing three density phases for the EAA–CNF-20 material, **b** 3D rendering of the (blue) high density fibre phase and the (green) low density phase. (Color figure online)

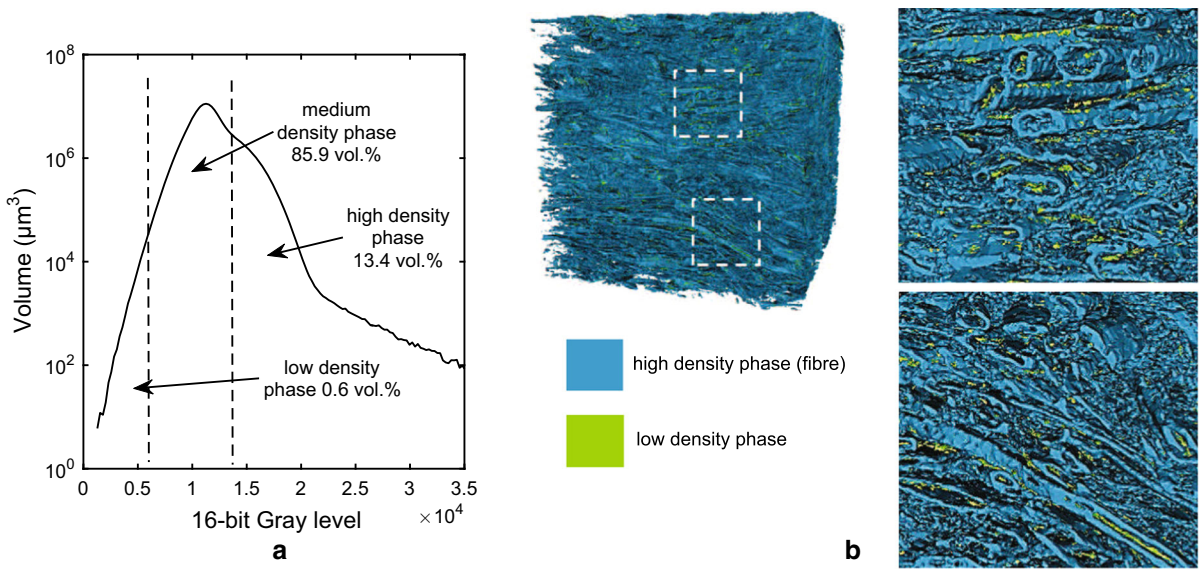

Fig. 5 EAA–pulp-20 **a** X-ray microtomography data showing three density phases for the EAA–Pulp-20 material, **b** 3D rendering of the (blue) high density fibre phase and the (green) low density phase

Table 2) formed gradually after compression moulding and the accuracy of this crystallinity was therefore uncertain since the time between compression moulding and DSC measurements was not the same for all samples. However, addition of cellulose to EAA did not significantly influence the primary crystallinity of EAA (X_{c2} in Table 2), which varied between 9 and 15% for the composite materials with no apparent trend. Previous works on cellulose composites have shown that cellulose reinforcement in composites can both induce and reduce crystallinity in the matrix phase (Samir et al. 2004; Yao et al. 2008; Maia et al. 2017). The crystallinity of EAA does not significantly change with the addition of cellulose, apart from a

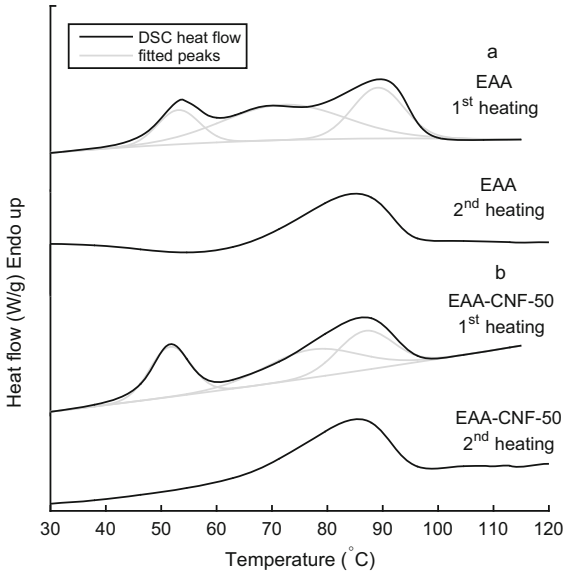

Fig. 6 Thermograms and fitted Gauss-peaks of the first and second heating scans for *a* neat compression moulded EAA, *b* EAA–CNF-50 composite

small reduction in crystallinity at higher cellulose contents, which suggests that any improvement in mechanical properties of the composites would probably be the result of the cellulose reinforcement and not due to the increased crystallinity of the EAA. The measured dynamic storage modulus and loss factor of the CNF–EAA composites over a broad temperature range are shown in Fig. 7. Three transitions can be discerned, the first at a temperature of $-39 \pm 4\,^{\circ}\mathrm{C}$, probably the glass transition temperature of the EAA matrix and a second transition at $55 \pm 5\,^{\circ}\mathrm{C}$, corresponding to the first melting temperature T_{m1} of the EAA matrix. The second melting peak, previously denoted as T_{m2} observed in the DSC analysis, is clearly seen by the loss factor, $\tan\delta$, for samples containing 0–30 vol% CNF, see Fig. 7b. Addition of CNF not only increased the magnitude of E' up to the melting at about 55 °C but also reduced the drop in E' after 55 °C, suggesting a general stiffening effect. The transitions decreased in magnitude with increasing CNF content, becoming insignificant above 40 vol% CNF.

Tensile properties

Typical stress-strain curves of the composites are shown in Fig. 8. Neat EAA was a highly ductile polymer with an elongation at break (ε_b) of about 500% and a low elastic modulus (E), see Table 3. The high ε_b of the EAA was significantly reduced by the addition of cellulose to the composites. As expected, the distinctive yield point seen in neat EAA at 13% strain disappeared when cellulose was added (see inset plot in Fig. 8). The cellulose composites instead showed a monotonous increase in stress until fracture. This behavior was observed for both CNF–EAA and pulp–EAA composites. Such deformation behavior has been attributed to deformation-induced rearrangements in the fibril/microfibril network (Ansari et al. 2014; Henriksson et al. 2008). In Fig. 9a, the Young's modulus of the CNF–EAA composites is shown as a function of cellulose volume fraction. The modulus

Table 2 Thermal properties of cellulose-EAA composites

Sample	Cellulose		$T_{m1} = 51 \pm 2\,^{\circ}\mathrm{C}$	$T_{m2} = 87 \pm 1\,^{\circ}\mathrm{C}$
	vol%	wt%	X_{c1} (%)	X_{c2} (%)
EAA	–	–	3	16
EAA–CNF-10	10	15	2	15
EAA–CNF-20	20	28.4	6	14
EAA–CNF-30	30	40.5	5	12
EAA–CNF-40	40	51.4	3	15
EAA–CNF-50	50	61.3	5	12
EAA–CNF-60	60	70.4	5	14
EAA–CNF-70	70	78.8	6	10
EAA–Pulp-20	20	28.4	7	12
EAA–Pulp-50	50	61.3	4	10
EAA–Pulp-70	70	78.8	3	9

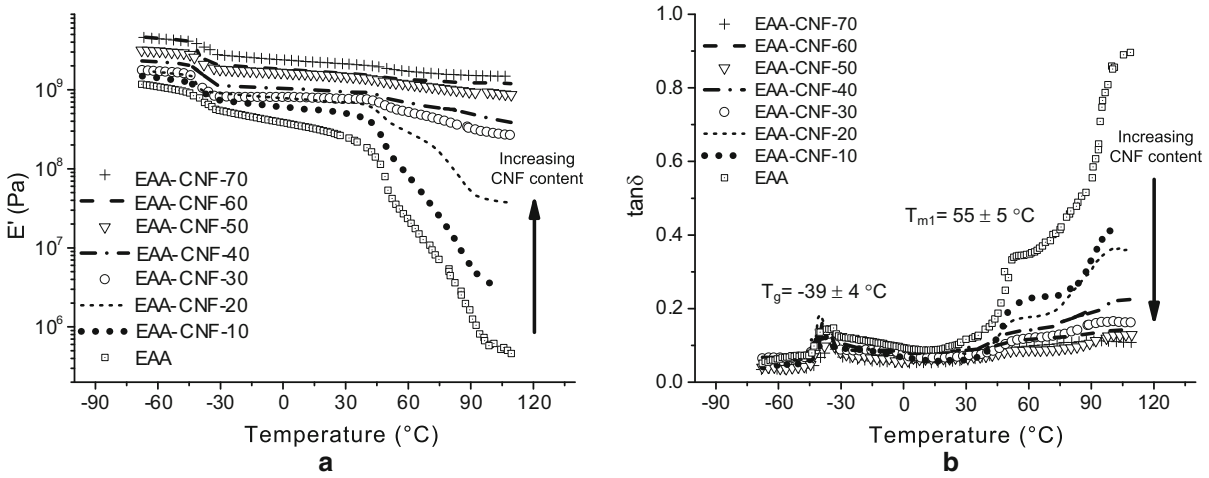

Fig. 7 **a** Storage modulus (E′) and **b** loss factor (tan δ) of the CNF–EAA nanocomposites studied in the temperature range from − 80 to 110 °C measured at a frequency of 1 Hz and a heating rate of 3 °C/min

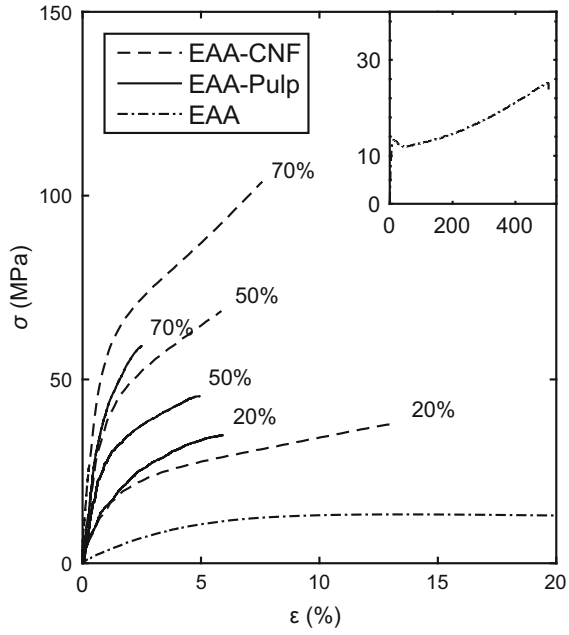

Fig. 8 Typical stress-strain curves of CNF–EAA and pulp–EAA composites. The inset shows the full stress–strain behavior for EAA

was observed to increase with increasing CNF content from 0.3 GPa for neat EAA to 6 GPa at 70 vol% CNF content, which gives a stiffening factor of 21. The Cox–Krenchel model in Fig. 9a was accurate at cellulose contents below 20 vol% and in the interval 40 to 60 vol%. The model underestimated the stiffness increase in the interval 20–40 vol%. The average fibril aspect ratio assumed in the model was however based on fibre analysis data which neglects both pulp fines and cellulose fibrils. Accurate modeling of the tensile properties would require more detailed knowledge about the fibril size and fibril content of the CNF. An increase in tensile properties of the CNF composites compared to those of the pulp composites could be expected since cellulose fibrils are known to have both a larger aspect ratio and a higher elastic modulus than pulp fibres (Tanpichai et al. 2012). The Cox–Krenchel model in Fig. 9b was accurate for the pulp–EAA composites, which was expected since this cellulose consisted mostly of pulp fibres and fibre analysis showed a lower fines content than the CNF.

A large reduction in effective stiffness $E_{f,l}$ with increasing CNF content has been linked to fibril aggregation in CNF composites (Ansari et al. 2014). The $E_{f,l}$ in Table 3, had a maximum value of 22.3 GPa for 30 vol% CNF, accompanied by a minor decrease to 18.6 GPa for 70 vol% CNF. This small decrease in effective stiffness suggests a small variation in dispersion of CNF in the EAA matrix in the range of 30–70 vol% CNF. Interestingly, the pulp composite were stiffer than the CNF composite at 20 vol% cellulose. The CNF composites had a stiffening threshold in the interval 20–30 vol% where the stiffness nearly doubled. This threshold concentration has been reported earlier in similar composites, Larsson et al. reported a significant stiffness increase in CNF/PLA composites at a cellulose concentration of 25 wt% (Larsson et al. 2012). Moreover, Maia et al.

Table 3 Tensile properties of cellulose-EAA composites

Sample	Tensile properties			Effective stiffness
	E (GPa)	σ_b (MPa)	ε_b (%)	$E_{f,l}$ (GPa)
EAA	0.3 ± 0.1	24 ± 1	491 ± 19	–
EAA–CNF-10	0.7 ± 0.1	26 ± 1	32 ± 5	9.4
EAA–CNF-20	1.6 ± 0.1	37 ± 1	14 ± 2	15.9
EAA–CNF-30	3 ± 0.4	57 ± 1	8 ± 1	22.3
EAA–CNF-40	4 ± 0.6	64 ± 12	8 ± 2	21.4
EAA–CNF-50	4.3 ± 0.3	65 ± 5	6 ± 1	19.0
EAA–CNF-60	5.3 ± 0.6	71 ± 11	5 ± 2	19.3
EAA–CNF-70	6.2 ± 0.3	83 ± 10	8 ± 1	18.6
EAA–Pulp-20	1.8 ± 0.5	35 ± 3	6 ± 1	18.6
EAA–Pulp-50	4.4 ± 1.2	46 ± 5	3 ± 1	19.5
EAA–Pulp-70	4.9 ± 0.2	55 ± 4	3 ± 0.3	13.7

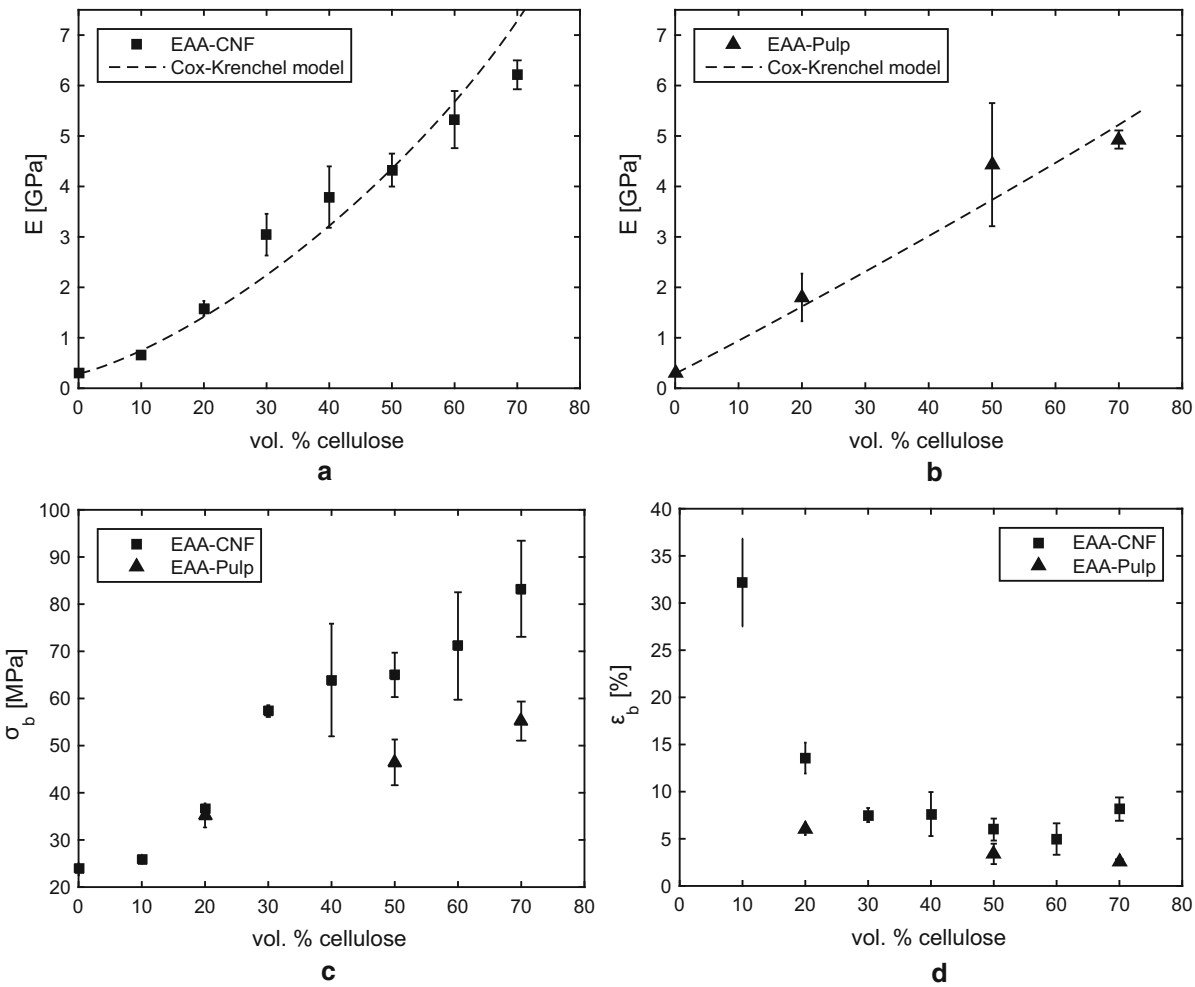

Fig. 9 Elastic modulus along with the Cox–Krenchel prediction for **a** CNF–EAA composites and **b** pulp–EAA composites, tensile properties for all cellulose composites **c** stress at break and **d** strain at break

reported a doubling of the stiffness to 0.67 GPa in the interval 20–30 wt% for CNF and elastomer composites (Maia et al. 2017). The strength σ_b of the CNF composites was also affected by this concentration threshold (Fig. 9c). The fibril network in the composites seem to have a percolation point where it can form entanglements and enhance both stiffness and strength greatly. The CNF composites produced were measured to have a significantly higher strength than the pulp composites at a cellulose content above 20 vol%. Such an increase in strength was expected from previous work on similar composites mixed in the dry state (Ariño and Boldizar 2012). The present results indicate that the water-assisted mixing method has the potential to be better than dry mixing. Both CNF and pulp mixed in the wet state led to an increased strength by a factor of 1.5 at 20 vol% cellulose (Table 3). The composite with the highest loading of 70 vol% CNF had a strength of 83.3 MPa which was an increase by a factor of 3.5 compared to the EAA matrix.

The strain at break (ε_b) decreased with the addition of CNF, the lowest value being about 5% for the 60 vol% composite and the highest being 32% for the 10 vol% composite. The pulp–EAA composites generally had somewhat lower ε_b than the CNF–EAA composites (Fig. 9d). This ability to withstand deformation was generally larger for CNF-containing than for pulp-containing composites, implying higher mobility of the fibrils than of the fibres under stress and a better matrix-to-cellulose stress transfer. The morhpology of both CNF and pulp composites suggested potential voids near the cellulose surface (Figs. 4, 5). Such voids would have a negative impact on both the stiffness and strength of the EAA composites since matrix-to-cellulose stress transfer would not be optimal. The removal of such near-surface voids would most likely increase the mechanical properties of the CNF and pulp composites even further.

Conclusions

The water assisted mixing method was found to be useful for preparing thermoplastic composites consisting of EAA copolymer reinforced with up to 70 vol% cellulose nanofibrils, departing from a 10% suspension of cellulose nanofibrils and a water-dispersed EAA copolymer. After drying and compression moulding, the cellulose fibrils were well dispersed in the EAA matrix as seen with X-ray computer tomography. Some voids were, however, found in the interface between cellulose and the EAA matrix, suggesting that the adhesion between the matrix and cellulose surfaces could be improved.

The addition of cellulose nanofibrils improved the mechanical properties of the composites substantially. The tensile stiffness increased with the cellulose nanofibril content, from 0.3 GPa for the neat EAA to 6 GPa for the composite with 70 vol% cellulose nanofibrils. A maximum in effective stiffness was found at 30 vol% nanofibrils content. The stiffness of the composite reinforced with a cellulose pulp was 5 GPa for 70 vol% pulp in EAA. The tensile strength of the composites reinforced with cellulose nanofibrils increased from 24 MPa for the neat EAA to 83 MPa for composite with 70% cellulose nanofibrils. The strength of composites reinforced with cellulose pulp was 55 MPa for the 70 vol% pulp composite, which was substantially lower than for the composites with cellulose nanofibrils. The elongation at break of the composites with 70 vol% cellulose nanofibrils was about 5%, being twice as high as for the corresponding cellulose pulp composite.

Acknowledgments The authors gratefully acknowledge the funding from the Swedish Foundation for Strategic Research. Author TM acknowledges the Knut and Alice Wallenberg Foundation through the Wallenberg Wood Science Center. Thanks are due to Dr. Assya Boujemaoui for performing carbohydrate analysis, to Jörgen Romild for help with tensile testing and to Dr. J. A. Bristow for the linguistic revision of the manuscript.

References

Ansari F, Galland S, Johansson M, Plummer CJ, Berglund LA (2014) Cellulose nanofiber network for moisture stable, strong and ductile biocomposites and increased epoxy curing rate. Compos Part A Appl Sci Manuf 63:35–44

Ariño R, Boldizar A (2012) Processing and mechanical properties of thermoplastic composites based on cellulose fibers

and ethylene-acrylic acid copolymer. Polym Eng Sci 52(9):1951–1957
Berglund LA, Peijs T (2010) Cellulose biocomposites from bulk moldings to nanostructured systems. MRS Bull 35(3):201–207
Boldizar A, Klason C, Kubát J, Näslund P, Sáha P (1987) Prehydrolyzed cellulose as reinforcing filler for thermoplastics. Int J Polym Mater 11(4):229–262
Brandrup J, Immergut E, Grulke E (1999) Polymer handbook, 4th edn. Wiley, Hoboken
Cox HL (1952) The elasticity and strength of paper and other fibrous materials. Br J Appl Phys 3(3):72
de Menezes AJ, Siqueira G, Curvelo AA, Dufresne A (2009) Extrusion and characterization of functionalized cellulose whiskers reinforced polyethylene nanocomposites. Polymer 50(19):4552–4563
Diddens I, Murphy B, Krisch M, Mller M (2008) Anisotropic elastic properties of cellulose measured using inelastic x-ray scattering. Macromolecules 41(24):9755–9759
Diniz JMBF, Gil MH, Castro JAAM (2004) Hornification: its origin and interpretation in wood pulps. Wood Sci Technol 37(6):489–494
Dufresne A (2017) Cellulose nanomaterial reinforced polymer nanocomposites. Curr Opin Colloid Interface Sci 29(Supplement C):1–8
Ehrnrooth E, Kolseth P (1984) The tensile testing of single wood pulp fibers in air and in water. Wood Fiber Sci 16:549–566
Favier V, Canova GR, Cavaill JY, Chanzy H, Dufresne A, Gauthier C (1995) Nanocomposite materials from latex and cellulose whiskers. Polym Adv Technol 6(5):351–355
Henriksson M, Berglund LA, Isaksson P, Lindström T, Nishino T (2008) Cellulose nanopaper structures of high toughness. Biomacromolecules 9(6):1579–1585
Jonoobi M, Harun J, Mathew A, Oksman K (2010) Mechanical properties of cellulose nanofiber (CNF) reinforced polylactic acid (PLA) prepared by twin screw extrusion. Compos Sci Technol 70(12):1742–1747
Larsson K, Berglund LA, Ankerfors M, Lindstrom T (2012) Polylactide latex/nanofibrillated cellulose bionanocomposites of high nanofibrillated cellulose content and nanopaper network structure prepared by a papermaking route. J Appl Polym Sci 125(3):2460–2466
Loo YL, Wakabayashi K, Huang YE, Register RA, Hsiao BS (2005) Thin crystal melting produces the low-temperature endotherm in ethylene/methacrylic acid ionomers. Polymer 46(14):5118–5124
Maia THS, Larocca NM, Beatrice CAG, de Menezes AJ, de Freitas Siqueira G, Pessan LA, Dufresne A, Frana MP, de Almeida Lucas A (2017) Polyethylene cellulose nanofibrils nanocomposites. Carbohydr Polym 173(Supplement C):50–56
Moberg T, Rigdahl M (2012) On the viscoelastic properties of microfibrillated cellulose (MFC) suspensions. Annu Trans Nord Rheol Soc 20:123–130
Naderi A, Lindström T, Sundström J (2014) Carboxymethylated nanofibrillated cellulose: rheological studies. Cellulose 21(3):1561–1571
Oksman K, Aitomäki Y, Mathew AP, Siqueira G, Zhou Q, Butylina S, Tanpichai S, Zhou X, Hooshmand S (2016) Review of the recent developments in cellulose nanocomposite processing. Compos Part A Appl Sci Manuf 83:2–18
Quennouz N, Hashmi SM, Choi HS, Kim JW, Osuji CO (2015) Rheology of cellulose nanofibrils in the presence of surfactants. Soft Matter 12:157–164
Saarikoski E, Lipponen S, Rissanen M, Seppälä J (2012) Blending cellulose with polyethylene-co-acrylic acid in alkaline water suspension. Cellulose 19(3):661–669
Saito T, Kimura S, Nishiyama Y, Isogai A (2007) Cellulose nanofibers prepared by TEMPO-mediated oxidation of native cellulose. Biomacromolecules 8(8):2485–2491
Samir MASA, Alloin F, Sanchez JY, Dufresne A (2004) Cellulose nanocrystals reinforced poly(oxyethylene). Polymer 45(12):4149–4157
Sehaqui H, Zhou Q, Berglund LA (2011) Nanostructured biocomposites of high toughness: a wood cellulose nanofiber network in ductile hydroxyethylcellulose matrix. Soft Matter 7:7342–7350
Siqueira G, Bras J, Dufresne A (2009) Cellulose whiskers versus microfibrils: Influence of the nature of the nanoparticle and its surface functionalization on the thermal and mechanical properties of nanocomposites. Biomacromolecules 10(2):425–432
Srithep Y, Turng LS, Sabo R, Clemons C (2012) Nanofibrillated cellulose (NFC) reinforced polyvinyl alcohol (PVOH) nanocomposites: properties, solubility of carbon dioxide, and foaming. Cellulose 19(4):1209–1223
Tanpichai S, Quero F, Nogi M, Yano H, Young RJ, Lindström T, Sampson WW, Eichhorn SJ (2012) Effective youngs modulus of bacterial and microfibrillated cellulose fibrils in fibrous networks. Biomacromolecules 13(5):1340–1349
Thomason J, Vlug M (1996) Influence of fibre length and concentration on the properties of glass fibre-reinforced polypropylene: 1. Tensile and flexural modulus. Compos Part A Appl Sci Manuf 27(6):477–484
Volk N, He R, Magniez K (2015) Enhanced homogeneity and interfacial compatibility in melt-extruded cellulose nanofibers reinforced polyethylene via surface adsorption of poly(ethylene glycol)-block-poly(ethylene) amphiphiles. Eur Polym J 72:270–281
Yao F, Wu Q, Lei Y, Xu Y (2008) Rice straw fiber-reinforced high-density polyethylene composite: effect of fiber type and loading. Ind Crops Prod 28(1):63–72
Zhang J, Chen S, Su J, Shi X, Jin J, Wang X, Xu Z (2009) Non-isothermal crystallization kinetics and melting behavior of eaa with different acrylic acid content. J Therm Anal Calorim 97(3):959–967